Crystallographic effects in micro/nanomachining of single-crystal calcium fluoride

Jiwang Yan[a)]
Micro/Nano Machining Laboratory, Department of Mechanical Engineering, Kitami Institute of Technology, Koen-cho 165, Kitami 090-8507, Japan

Katsuo Syoji
Department of Mechatronics and Precision Engineering, Tohoku University, Aramaki-Aoba-01, Aoba-ku, Sendai 980-8579, Japan

Jun'ichi Tamaki
Micro/Nano Machining Laboratory, Department of Mechanical Engineering, Kitami Institute of Technology, Koen-cho 165, Kitami 090-8507, Japan

(Received 30 April 2003; accepted 20 October 2003; published 24 December 2003)

Single-crystal calcium fluoride (CaF_2) is an excellent optical material in the infrared range and the ultraviolet range. It is an indispensable substrate material for the 193 and 157 nm wavelength laser optics for future large-scale semiconductor photolithography systems. Due to its delicate nature, for the most part the CaF_2 elements have been fabricated using conventional pitch polishing combined with interferometry and local surface correction to form the desired flat, sphere or aspherical surface. In the present work, the feasibility of generating high quality optical surfaces on CaF_2 by single-point diamond turning is examined. The development of this technology may provide the possibility of fabricating aspherical and diffractive optical components in an efficient way. The machining experiments described in this article were done on a high-stiffness, ultraprecision, numerically controlled diamond lathe with a sharply pointed single-crystal diamond tool. The scale of machining was varied from the micrometer level to the nanometer level. It was found that at the micrometer level, machining was significantly affected by the crystal orientation of the workpiece. The crystallographic anisotropy causes nonuniformity of the finished surface texture, microfracture topography and brittle–ductile transition boundary conditions. The results also indicate that by controlling the undeformed chip thickness below a critical value, namely, the minimum critical chip thickness (85 nm), a uniformly ductile-machined surface could be produced. Under the present experimental conditions, a surface with a maximum height (Ry) of 18.5 nm and arithmetical mean roughness (Ra) of 3.3 nm was obtained. © *2004 American Vacuum Society.*
[DOI: 10.1116/1.1633770]

I. INTRODUCTION

Calcium fluoride (CaF_2) is a transparent colorless crystal with a fluorite-type crystalline structure. It has extremely high permeability and a refractive index from the infrared range to the ultraviolet range and excellent color-aberration compensation capability. Therefore, CaF_2 is not only an optical substrate material for infrared imaging systems, but also an indispensable lens substrate material for future large-scale semiconductor photolithography systems. With 193 and 157 nm lithography systems being developed and CaF_2 components utilized to replace fused silica (SiO_2), CaF_2 is becoming the most commercially important material within the optics community. Fused SiO_2, the primary optical material used for 248 and 193 nm lithography, has more than 99%/cm of bulk transmission at 193 nm; at 157 nm, however, its transmission drops to less than 5%/cm. On the other hand, CaF_2 has bulk transmission greater than 98%/cm at 157 nm. Currently, CaF_2 is the only robust highly developed material with sufficient transmissibility at 157 nm. Specific applications for CaF_2 include 193 nm excimer laser components, chromatic aberration correction of 193 nm stepper lens systems, and stepper lenses for future 157 nm systems. Some of these CaF_2 elements have already been fabricated for prototype and preproduction lithographic lenses.[1]

The optical performance of CaF_2 is strongly influenced by its surface quality. As shown by previous reports, laser damage performance for CaF_2 is strongly dependent on preparation of the surface[2] and the transmission performance for CaF_2 depends on the surface roughness.[3] On the other hand, CaF_2 is nominally a brittle material, with very low toughness to fracture, low hardness and a very high thermal-expansion coefficient. Due to these drawbacks CaF_2 is very difficult to machine for high quality optical surfaces. For the most part CaF_2 optical elements have been fabricated using conventional pitch polishing combined with interferometry and local surface correction, by hand or computer controlled, to form the desired flat, sphere or aspherical surface. This technique is successful when the workpiece material is amorphous, but fails when polishing single-crystal CaF_2, since its hardness is dependent on crystal orientation making material removal anisotropic. Normal polishing thus results in a lobed structure with three high zones and three low zones for the

[a)]Corresponding author; electronic mail: yanjw@mail.kitami-it.ac.jp

Downloaded from Yan Laboratory, Keio University at http://www.yan.mech.keio.ac.jp. Redistribution is subject to copyright licence from the journal publisher.

{111} crystal surface.[4] For this reason, it becomes difficult to polish surfaces with small figure errors, particularly steeply curved surfaces such as aspherical and diffractive optical elements, which are required more and more in recent optical systems for system miniaturization and improvement of image quality.[5]

An alternative polishing method called magnetorheological finishing (MRF) has been developed to overcome the limitations of traditional pitch polishing techniques.[4,6] In MRF, material is removed by hydrodynamic forces generated by the flow of a magnetorheological fluid. By modifying the dwelling time or removal rate at each point on the surface to compensate for variations in material properties, MRF can produce extremely accurate optical surfaces on CaF_2.[4,6]

Another alternative method for machining CaF_2 is single-point diamond turning (SPDT). SPDT is capable of ultraprecision machining of optical components that have both complex shape and high accuracy. This technology requires the use of extremely rigid, ultraprecise, numerically controlled machine tools under strict environmental control, and single-point diamond tools with extremely sharp cutting edges. Conventionally, SPDT has been used to machine ductile nonferrous metal materials for mirrors and prisms, and so on.[7] Recently, a few semiconductor substrates, such as silicon and germanium, have also been demonstrated to be machinable by SPDT.[8–15] However, to date, little focus has been placed on the single-point diamond turning of CaF_2.

In the present work, we conducted single-point diamond machining experiments on CaF_2 on the micrometer/nanometer level machining scale in order to examine possible conditions for fabricating high-quality optical surfaces. Because CaF_2 is a highly brittle single-crystalline material with strong crystallographic anisotropy, the microscopic mechanical properties vary with the crystal orientations, and result in significantly different processing behavior. The crystallographic effect will cause nonuniformity in surface quality and eventually limit productivity of the machining process. Therefore, in this study, we primarily investigated the effects of the crystal orientation on the machining mechanisms.

II. EXPERIMENTAL PROCEDURES

Single-point diamond turning experiments were carried out on a three-axis numerically controlled ultraprecision diamond lathe that has an air-bearing spindle, two perpendicular hydrostatic-bearing linear tables and a hydrostatic-bearing rotary table. Laser scales were used in the machine to measure and control displacement of the tables, thus enabling motion resolution of 10 nm per step. A schematic of the machining setup is shown in Fig. 1(a).

A straight-nosed cutting tool made of single-crystal diamond was used in the experiments. The cutting model is shown in Fig. 1(b). The undeformed chip thickness (h), that is, the thickness of the work material to be removed per revolution of workpiece, is independent of the depth of cut (a), and is determined by the tool feed (f) and cutting edge angle (κ), according to

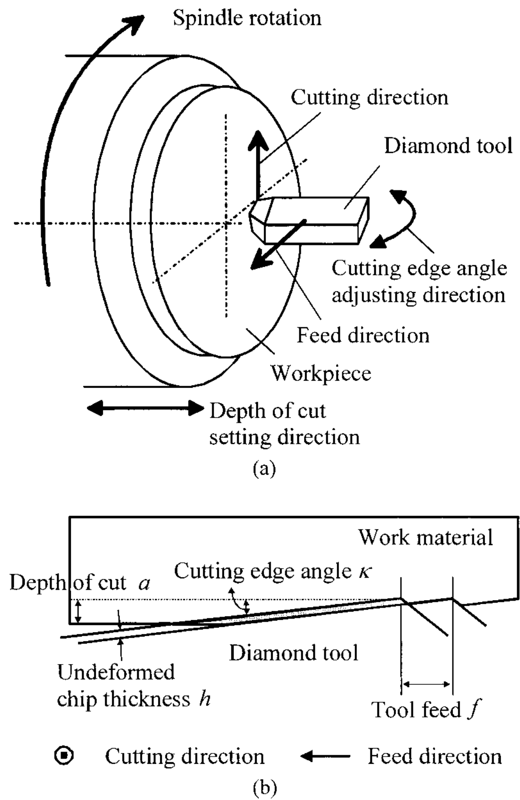

FIG. 1. Schematics of (a) the single-point diamond turning setup and (b) the machining model.

$$h = f \sin \kappa. \quad (1)$$

It can be seen that there is a trade-off between f and $\sin \kappa$. That is, one may use either a small tool feed or a small cutting edge angle to obtain an extremely small undeformed chip thickness. Usually, it is industrially beneficial to use a small cutting edge angle rather than a small tool feed for high machining efficiency.[13] By using a sufficiently small cutting edge angle, it is possible to thin the undeformed chip thickness to the nanometric range over the entire region of cutting, enabling ductile regime machining of brittle materials.

Single-crystal CaF_2 specimens with (111) surface orientation and dimensions of 50 mm diameter and 5 mm thickness were used as workpieces. The workpieces were prepolished to remove existing microcracks and bonded on diamond-turned aluminum blanks using 50 °C heat-softened glue and then vacuum chucked to the machine spindle. The rake angle of the diamond tool was −20°, and the relief angle was 6°. The tool rake angle is the angle between the leading edge of a cutting tool and the perpendicular of the surface being cut. If the leading edge of the blade is behind the perpendicular of the surface being cut, the angle is positive; if the leading edge of the blade is ahead of the perpendicular, the angle is negative. Generally, tools with positive rake angles are used when cutting ductile metals. The purpose of using a negative rake angle tool in this work is to generate a high hydrostatic pressure region ahead of and beneath the tool, which is essential for ductile mode removal of brittle materials.[8]

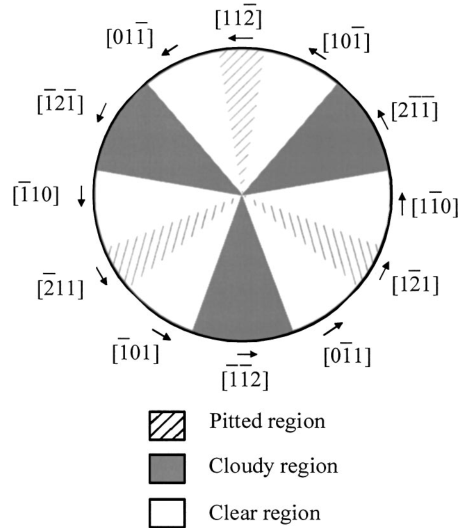

FIG. 2. Schematic of the CaF_2 (111) surface machined at undeformed chip thickness of 1 μm. The numerals and arrows indicate the crystal orientations along the corresponding cutting directions.

The undeformed chip thickness was changed from a few nanometers to 1.5 μm by varying the tool feed from 1 to 60 μm/rev and the cutting edge angle from 0.1° to 1.5°. The depth of cut was varied between 1 and 5 μm. The spindle rotation rate was constant at 1500 rpm. Face turning was performed, with a corresponding cutting speed of 0–235.5 m/min. In order to avoid the influence of thermal effects[16] and possible chemical effects on the machining process, no coolant was used, and dry cuts were performed.

The machined surfaces were examined using a Nomarski differential interference microscope and a scanning electron microscope (SEM), and measured using a surface profiler, Form TalySurf, and an atomic force microscope (AFM). The chips removed from the workpieces during machining were collected and observed with the SEM.

III. RESULTS AND DISCUSSION

A. Crystallographic effect on surface texture

First, the effect of crystal orientation on the machined surface texture was examined. A facing cut was performed at a tool feed of 60 μm/rev, a cutting edge angle of 1° and a depth of cut of 5 μm. Under these conditions, the undeformed chip thickness was approximately 1 μm. Figure 2 shows a schematic of the machined surface. The surface texture differs significantly according to the crystal orientation. There are six damaged regions distributed in a radial pattern from the workpiece center. Three arms of slightly pitted regions are observed along the $[11\bar{2}]$, $[1\bar{2}1]$, and $[\bar{2}11]$ orientations and three arms of cloudy regions are along the $[2\bar{1}\bar{1}]$, $[\bar{1}2\bar{1}]$, and $[\bar{1}\bar{1}2]$ orientations, whereas the six $\langle\bar{1}01\rangle$ orientations corresponded to damage-free clear regions.

Next, detailed SEM observations were performed on various orientations of the workpiece in order to examine the microfracturing mechanism. Figures 3(a)–3(c) are SEM photographs of the machined surfaces along the $[11\bar{2}]$, $[\bar{1}\bar{1}2]$, and $[\bar{1}01]$ orientations, respectively, corresponding to the three types of regions in Fig. 2. In Fig. 3(a), microfractures of up to a few tens of micrometers in size are observed, and most of the microfractures appear to be triangular. Cross-sectional surface profiling results showed that the depth of the microfractures averages in the range of 5–10 μm, far larger than the undeformed chip thickness (1 μm). In Fig.

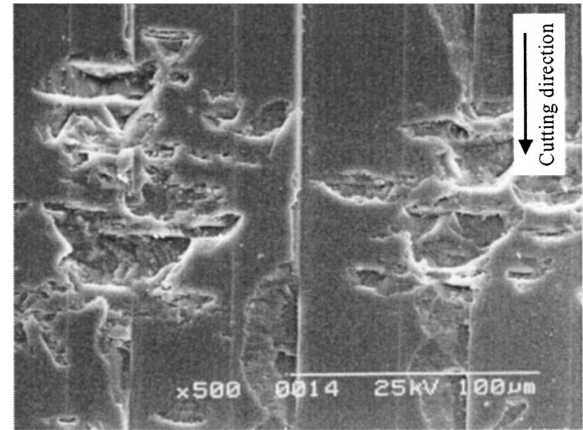

(a)

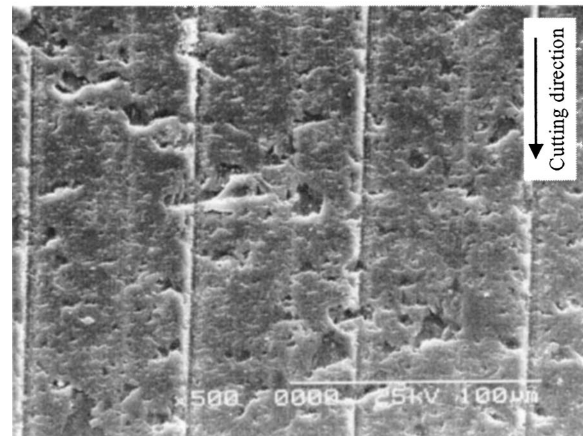

(b)

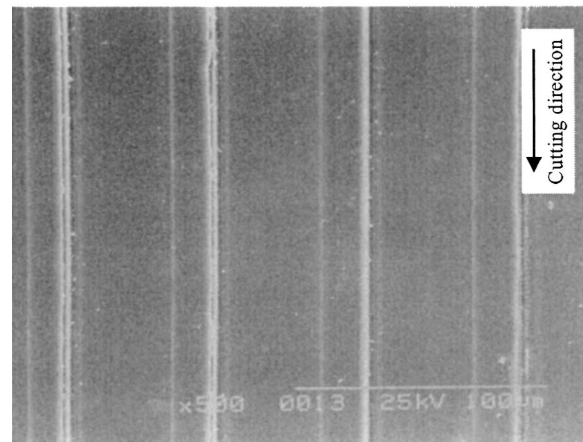

(c)

FIG. 3. SEM photographs of the three types of surface regions shown in Fig. 2. (a) $[11\bar{2}]$, pitted region; (b) $[\bar{1}\bar{1}2]$, cloudy region; (c) $[\bar{1}01]$, clear region.

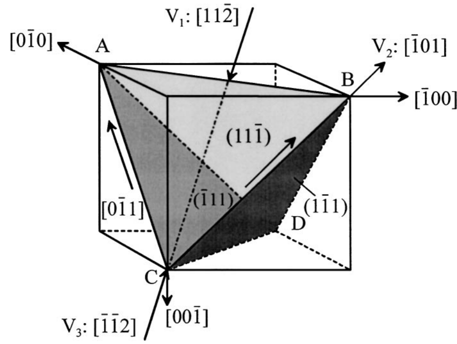

FIG. 4. Schematic indicating the relationships among the cutting directions, the cleavage planes and the slipping systems during machining of the CaF_2 (111) workpiece.

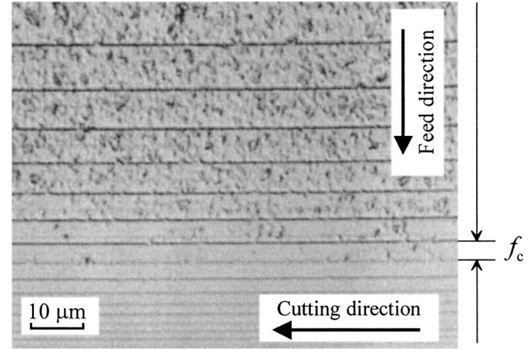

FIG. 5. Nomarski micrograph of the surface machined along $[\bar{1}\bar{1}2]$ under a continuously varied tool feed. Critical tool feed f_c can be identified at the brittle–ductile transition boundary.

3(b), microfractures are more dense, but the size and the depth of the microfractures are distinctly smaller than those in Fig. 3(a). In addition, the contours of the microfractures are twisted, and exhibit a plastic flow appearance. However, in Fig. 3(c), the entire surface is smooth, with periodical tool feed marks but no microfractures.

Because other conditions are the same, there is no doubt that the above differences in surface texture are caused by the crystallographic effect. As shown in Fig. 1(a), the cutting direction always changes with respect to the crystal orientations as the workpiece rotates. Consequently, the direction of the principal cutting force changes with respect to the orientations of the slipping systems and the cleavage planes of the crystal. The resolved tensile/shear stress acting on the cleavage/slipping planes changes during machining, and the behavior of these cleavage/slipping planes determines whether brittle fracture or plastic deformation occurs.

CaF_2 has a fluorite-type crystal structure, in which the cleavage plane is $\{111\}$ and the preferred slip system is $\{001\}\langle 1\bar{1}0\rangle$.[17] The relationships among the cutting directions, cleavage planes and slipping systems are schematically shown in Fig. 4. In Fig. 4, the surface to be cut is parallel to the (111) plane (*ABC*). V_1, V_2, and V_3 indicate the cutting directions along $[11\bar{2}]$, $[\bar{1}01]$, and $[\bar{1}\bar{1}2]$, respectively. As is known from the cutting principles, the principal cutting force, whose direction coincides with the cutting direction, dominates the material removal mechanism. When cutting along $[11\bar{2}]$ (V_1), the resolved tensile stress acting on the cleavage plane $(11\bar{1})$ (*ADB*) becomes predominant; hence, brittle fracture will immediately occur along these planes. The triangular microfractures shown in Fig. 3(a) are thought to have formed along the cleavage planes $(11\bar{1})$, $(\bar{1}11)$, and $(1\bar{1}1)$ (*ABD*, *ACD*, and *BCD*). When cutting along $[10\bar{1}]$ (V_2), the shear stress acting on the slip system (010) $[10\bar{1}]$ becomes predominant. According to Schmid law, this slipping system is liable to be activated; thus, slipping deformation occurs, leading to a ductile mode surface as shown in Fig. 3(c). However, when cutting along $[\bar{1}\bar{1}2]$ (V_3), two slip systems, $(010)[10\bar{1}]$ and $(100)[0\bar{1}1]$, become symmetrical to the cutting condition. In such a case, slipping may occur, but the slipping deformation along the two symmetrical slipping systems will be restricted by each other due to their intersection. A similar phenomenon has been confirmed in a transmission electron microscopic (TEM) investigation of the subsurface damage layer of silicon wafers generated by diamond turning.[18] The restriction between two symmetrical slipping systems results in a decrease in the microscopic ductility of work material. Therefore, the material removal mechanism along the $[\bar{1}\bar{1}2]$ orientation may involve both the restricted slipping along the two symmetrical slipping systems and the cleavage fracture along the $(11\bar{1})$ (*ADB*) plane, which would lead to the surface texture shown in Fig. 3(b).

B. Crystallographic effect on a brittle–ductile transition boundary

Crystal orientation influences the degree of priority between slipping deformation and cleavage fracture, thus it determines the ductile machinability. The ductile machinability of a brittle material can be represented by the critical chip thickness (alternately termed the critical depth, d_c), which is the maximum value of the undeformed chip thickness for achieving ductile material removal. In the present experiments, the value of d_c was measured by performing face turning under a continuously varied tool feed f at constant cutting edge angle κ. In this way, the critical tool feed f_c at which the brittle–ductile transition occurs can be identified. Then d_c can be calculated from f_c according to the relationship described in Eq. (1).

Figure 5 is a Nomarski micrograph of the surface machined along $[\bar{1}\bar{1}2]$ with the above method. Cutting edge angle κ was kept constant at 1.5°. From top to bottom of the photograph, the tool feed decreases continuously. As the tool feed decreases, both the number and the size of the microfractures keep decreasing and the critical tool feed at which microfractures began to disappear is $f_c = 5.5\ \mu$m/rev. The critical chip thickness d_c calculated from f_c is 140 nm.

These measurements were also performed on other orientations of the workpiece. Figure 6 is a Nomarski micrograph of the surface located between $[\bar{1}\bar{1}2]$ and $[\bar{1}01]$. It is evident that the critical tool feed, indicated by the brittle–

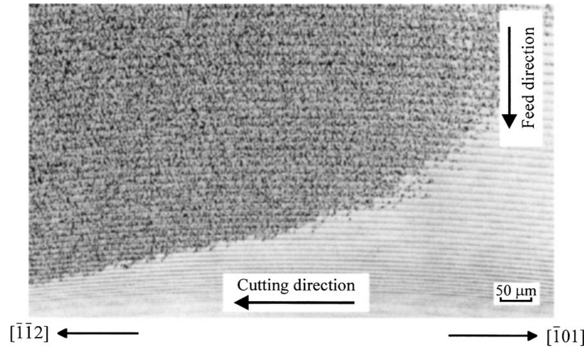

FIG. 6. Nomarski micrograph of the surface between $[\bar{1}\bar{1}2]$ and $[\bar{1}01]$, machined under a continuously varied tool feed.

ductile boundary, changes significantly with the crystal orientation. Figure 7 shows a plot of the critical chip thickness d_c versus the crystal orientation during one revolution of the workpiece. In Fig. 7, periodical variations of d_c can be observed. Six peaks, three deep valleys and three shallow valleys, appear during one revolution of the workpiece. The peaks occur at the $\langle 0\bar{1}1\rangle$ orientations, corresponding to the clear regions in Fig. 2. The shallow valleys appear at the $\langle \bar{1}\bar{1}2\rangle$ orientations, corresponding to the cloudy regions in Fig. 2; the deep valleys occur at the $\langle 11\bar{2}\rangle$ orientations, corresponding to the pitted regions in Fig. 2. The maximum critical chip thickness at the peaks is 1.2 μm, and the minimum critical chip thickness ($d_{c\ \min}$) at the deep valleys is 85 nm.

C. Ductile machining for a uniform surface

For optical applications, a machined surface must be uniform and completely damage free. These requirements can be satisfied by decreasing the undeformed chip thickness below the minimum critical chip thickness $d_{c\ \min}$, as indicated in Fig. 7. Such an extremely small undeformed chip thickness can be immediately achieved by adopting a sufficiently small cutting edge angle κ and/or a sufficiently small tool feed f, as can be seen in Fig. 1(b) and Eq. (1).

Figure 8 is a Nomarski micrograph of the CaF_2 surface

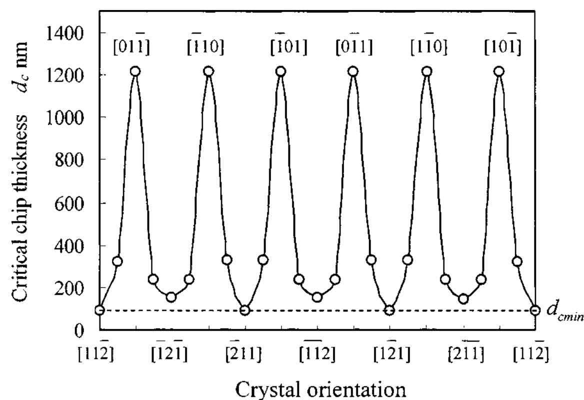

FIG. 7. Plot of the critical chip thickness vs the crystal orientation during one revolution of the CaF_2 (111) workpiece.

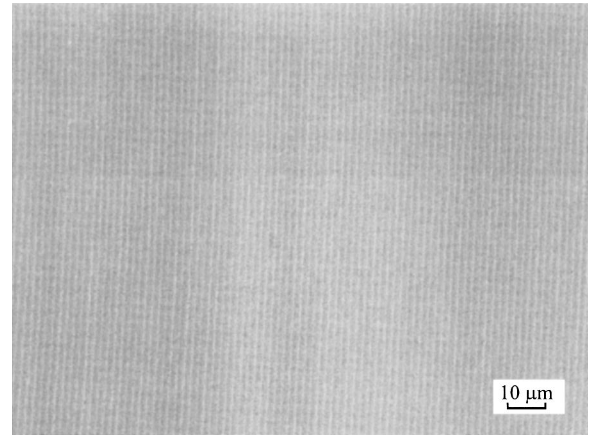

FIG. 8. Nomarski micrograph of the CaF_2 (111) surface machined at an undeformed chip thickness of 17 nm.

machined under conditions of $\kappa = 0.5°$, $f = 2\ \mu$m/rev and $a = 1\ \mu$m. These conditions determine an undeformed chip thickness of 17 nm. Under these conditions, the machined surface exhibits uniformity in texture, with no microfractures across the entire surface. Figure 9 is an AFM image of the same surface. Periodical tool-feed marks left by the diamond tool can be observed, but no microfracture is seen. The maximum height, namely, the peak to valley (Ry), of the surface is 18.5 nm, and the arithmetical mean surface roughness (Ra) is 3.3 nm, respectively. Figure 10 is a SEM photograph of the chips removed from the CaF_2 workpiece during the above machining process. The chips are generally continuous and partially curled, similar to the chips generated when cutting ductile metals at the nanometric level.[19] The appearance of these chips indicates that CaF_2, nominally a brittle material, has been removed from the workpiece in a completely ductile manner.

The above results demonstrate an important fact, i.e., that the crystallographic anisotropy effect in the material removal behavior can be significantly eliminated by decreasing the undeformed chip thickness to the range of a few tens of nanometers. This phenomenon is due to the size effect in the

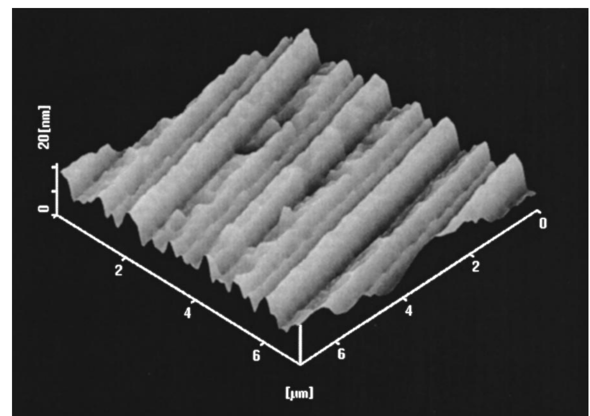

FIG. 9. AFM image of the topography of the surface shown in Fig. 8. The surface has a maximum height (Ry) of 18.5 nm and arithmetical mean roughness (Ra) of 3.3 nm, respectively.

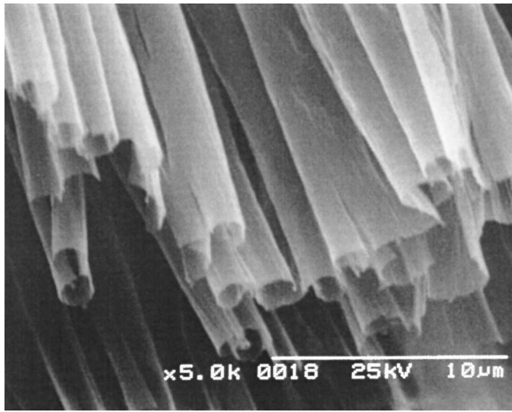

FIG. 10. SEM photograph of CaF_2 chips generated during the machining process.

brittle–ductile transition. That is, when the undeformed chip thickness is in the range of a few tens of nanometers, it will be as small as the edge radius of a commonly used diamond tool.[20] Under such conditions, the effective rake angle caused by the edge radius becomes a much higher negative value than the nominal tool rake angle. As a result, very high hydrostatic pressure will be generated in the cutting region ahead of and beneath the cutting tool.[13,21] It is this high hydrostatic pressure that makes a nominally brittle material plastically deformed and able to be removed in ductile mode, rather than fractured in a brittle manner.[22] Under the high hydrostatic stress state, the resolved tensile stress on the cleavage planes of the crystal will be significantly counteracted and become insufficient to cause cleavage fracture. Therefore, the behavior of the active slipping systems will dominate the material removal mode despite the change in crystal orientation. It can also be assumed that the edge radius of a cutting tool will also affect the anisotropic behavior in material removal, and, in turn, influence the minimum critical chip thickness $d_{c\min}$. Therefore, it may be beneficial to use a tool with a certain edge radius, that is, an appropriately blunt tool, rather than an extremely sharp tool, for better machining performance. These aspects will be investigated experimentally in the future.

IV. CONCLUDING REMARKS

Single-crystal calcium fluoride was machined at the micrometer-nanometer level using an ultrarigid, ultraprecise diamond lathe and a single-point diamond tool. It was found that in micrometer-level machining, the finished surface texture and the microfracture were significantly affected by the workpiece crystal orientation. Three types of surface regions with distinctly different formation mechanisms were identified. However, the investigation results for the brittle–ductile transition boundary conditions indicate that it is possible to achieve a uniformly ductile-cut surface despite the crystal orientations by using a sufficiently small undeformed chip thickness. The minimum critical chip thickness for fabricating a completely ductile-cut surface on CaF_2 (111) was 85 nm. Under this condition, the generation of optical surfaces with nanometric roughness is possible. Based on the present experimental conditions, a surface with a maximum height (*Ry*) of 18.5 nm and an arithmetical mean roughness (*Ra*) of 3.3 nm was obtained.

ACKNOWLEDGMENTS

This work was carried out as part of the project, Development of a New Ductile Machining Technology for the Fabrication of CaF_2 Aspherical Optics, funded by the Japan New Energy and Industrial Technology Development Organization (NEDO), Project No. 01A38004. The Grant-in-Aid for Young Scientists (Grant No. 15760073) from the Ministry of Education, Science, Sports and Culture of Japan, and grants from the Suzuki Scientific Foundation, are acknowledged. One of the authors (J.Y.) would also like to extend his gratitude to M. Negishi of the Core Technology Center, Nikon Corporation, and to H. Ito of the Production Engineering Department, Olympus Optical Co. Ltd., for their valuable information.

[1]V. Liberman, T. M. Bloomstein, M. Rothschild, J. H. C. Sedlacek, R. S. Uttaro, A. K. Bates, C. V. Peski, and K. Orvek, J. Vac. Sci. Technol. B **17**, 3273 (1999).
[2]E. Stenzel, S. Gogoll, J. Sils, M. Huisinga, H. Johansen, G. Kastner, M. Reichling, and E. Matthias, Appl. Surf. Sci. **109–110**, 162 (1997).
[3]R. S. Retherford, R. Sabia, and V. P. Sokira, Appl. Surf. Sci. **183**, 264 (2001).
[4]D. Golini, M. DeMarco, W. Kordonski, and J. Bruning, Laser Focus World **37**, 7 (2001).
[5]D. C. O'Shea, *Element of Modern Optical Design* (Wiley, New York, 1985).
[6]S. Arrasmith and S. D. Jacobs, LLE Review, Laboratory for Laser Energetics, University of Rochester, 1999, Vol. 80, pp. 213–219.
[7]N. Ikawa, R. R. Donaldson, R. Komanduri, W. Konig, P. A. McKeown, T. Moriwaki, and I. F. Stowers, Ann. CIRP **40**, 587 (1991).
[8]J. Yan, M. Yoshino, T. Kuriyagawa, T. Shirakashi, K. Syoji, and R. Komanduri, Mater. Sci. Eng., A **297**, 230 (2001).
[9]P. N. Blake and R. O. Scattergood, J. Am. Ceram. Soc. **73**, 949 (1990).
[10]T. Nakasuji, S. Kodera, S. Hara, H. Matsunaga, N. Ikawa, and S. Shimada, Ann. CIRP **39**, 89 (1990).
[11]W. S. Blackly and R. O. Scattergood, Precis. Eng. **13**, 95 (1991).
[12]D. A. Lucca, P. Chou, and R. J. Hocken, Ann. CIRP **47**, 475 (1998).
[13]J. Yan, K. Syoji, T. Kuriyagawa, and H. Suzuki, J. Mater. Process. Technol. **121**, 363 (2002).
[14]J. C. Morris, D. L. Callahan, J. Kulik, J. A. Patten, and R. O. Scattergood, J. Am. Ceram. Soc. **78**, 2015 (1995).
[15]K. E. Puttick, L. C. Whitmore, C. L. Chao, and A. E. Gee, Philos. Mag. A **69**, 91 (1994).
[16]J. Yan, K. Syoji, T. Kuriyagawa, K. Tanaka, and H. Suzuki, Proceedings of the ASPE 2000 Annual Meeting, Scottsdale, AZ, 22–27 October 2000, Vol. 22, pp. 66–69.
[17]R. W. Hertzberg, *Deformation and Fracture Mechanics of Engineering Materials* (Wiley, New York, 1983).
[18]T. Shibata, S. Fujii, E. Makino, and M. Ikeda, Precis. Eng. **18**, 129 (1996).
[19]N. Ikawa, S. Shimada, and H. Tanaka, Nanotechnology **3**, 6 (1992).
[20]I. Miyamoto, T. Ezawa, and K. Nishimura, Nanotechnology **1**, 44 (1990).
[21]J. Yan, K. Syoji, and T. Kuriyagawa, J. Jpn. Soc. Precis. Eng. **65**, 1008 (1999).
[22]P. W. Bridgman, J. Appl. Phys. **18**, 246 (1947).